Supplementary Information

Superhydrophobic inkjet printed flexible graphene circuits via direct-pulsed laser writing

Suprem R. Das[a,b,c], Srilok Srinivasan[a], Loreen R. Stromberg[a], Qing He[a], Nathaniel Garland[a], Warren E. Straszheim[d], Pulickel M. Ajayan [e], Ganesh Balasubramanian[f], Jonathan C. Claussen[a,b,c, *]

[a] Department of Mechanical Engineering, Iowa State University, Ames IA 50011

[b] Division of Materials Science and Engineering, Ames Laboratory, Ames IA 50011

[c] Applied Sciences Complex I and Microelectronics Research Center, Iowa State University, Ames 50011

[d] Materials Analysis and Research Laboratory, Iowa State University, Ames IA 50011

[f] Department of Mechanical Engineering and Mechanics, Lehigh University, Bethlehem, PA 18015

Corresponding Author Email: jcclauss@iastate.edu

Molecular Dynamics (MD) simulations

Due to the intrinsic size limitation of MD, simulating a water droplet sufficiently large for the line tension force at the contact line to be negligible is not practical. Hence, the value of the contact angle (CA) calculated from MD, in general, has some size dependence. We therefore adopt a semi-infinite cylindrical slab of water droplet in which the simulation box is narrow in the y-direction compared to the x and z direction[1, 2]. Size dependence of the contact angle thus calculated using this approach has been shown to be negligible[2].The size of our simulation box is a $25.84 \times 3.83 \times 20$ nm^3 with 4,000 water molecules arranged in a periodic-cube placed on top of a graphitic substrate. The simulation box is periodic in x and y direction while it has a fixed

boundary along the z-direction. Figure S1a shows an example of the starting configuration where the substrate is horizontally oriented for few layer graphene. The equilibrated system is shown in Figure S2, where the contact line is straight and hence the line tension contribution is zero due to the infinite curvature. We use the rigid simple extended point charge (SPC/E) model,[3] for the interactions between water molecules. In the SPC/E model, the O-H bonds and the H-O-H angles are considered rigid. The water molecules interact with each other via Coulombic interactions and 12-6 Lennard Jones (LJ) interaction between the oxygen atoms. The parameters used for the SPC/E model is listed in Table 1.

Table 1: Parameters for SPC/E water model

Parameters	**Value**
Charge on Oxygen, Q_o	-0.8476
Charge on hydrogen, Q_H	0.4238
ε_{O-O}	0.650 kJ mol^{-1}
σ_{O-O}	3.166 Å

The cut-off for the LJ interactions and the short range Coulombic interactions between the water molecules is 10 Å. The long range Coulombic interactions were computed in k-space using the particle-particle particle-mesh (PPPM) solver[4]. Since the simulation box is non-periodic in the z-direction we introduce an artificial reflecting wall on top edge of the simulation box to prevent water molecules from escaping the simulation box. For the purpose of computing the long range Coulombic interactions, the PPPM solver treats the system as if it was periodic in z direction while inserting an empty volume between the periodic images and turning off the interactions between the periodic images in the z direction[5]. The ratio of the extended z dimension to the initial z dimension was set as 3.

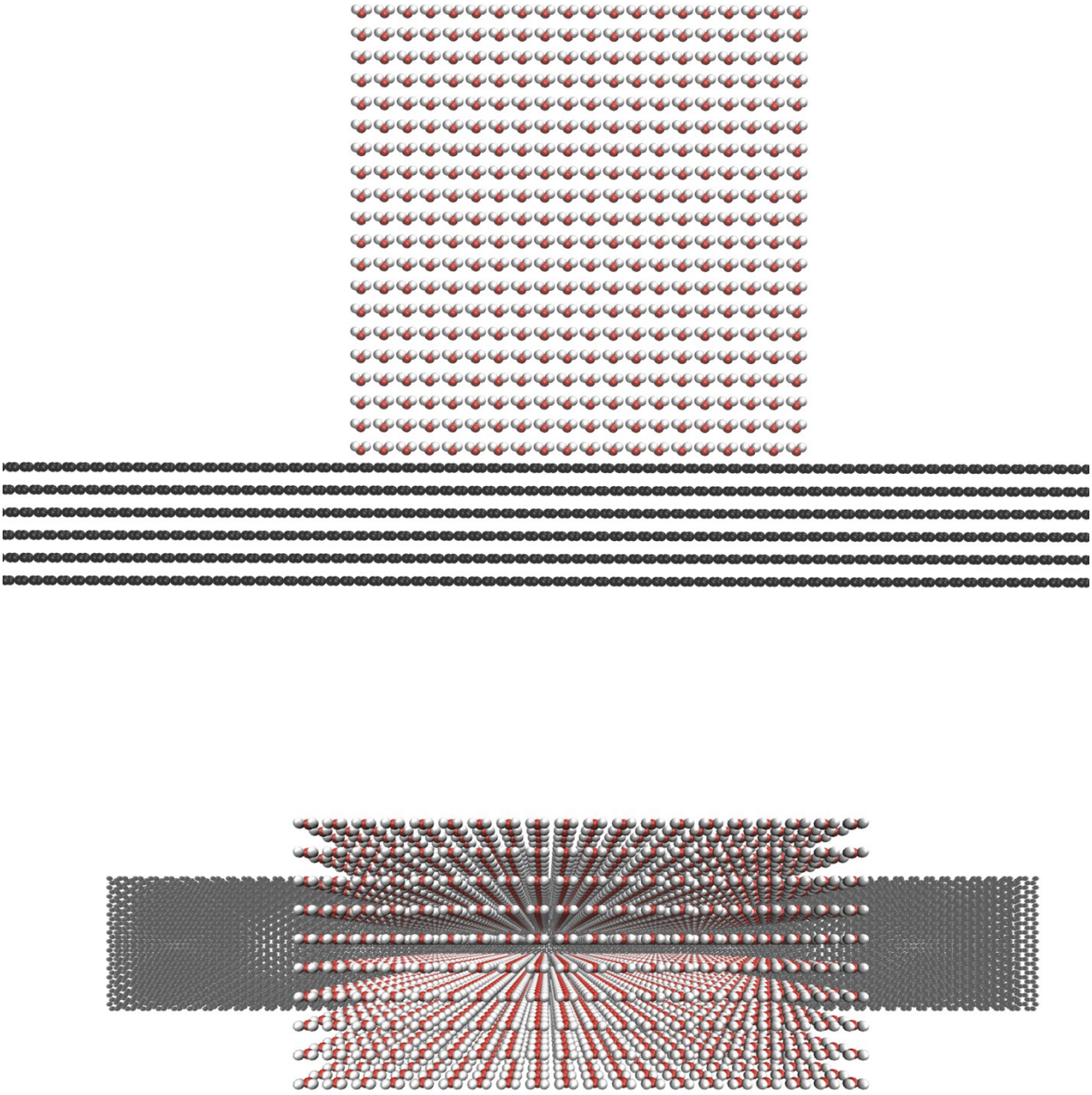

Figure S1: (Top) Side view of the initial configuration of the simulation box and **(Bottom)** top view of the initial configuration of the simulation box

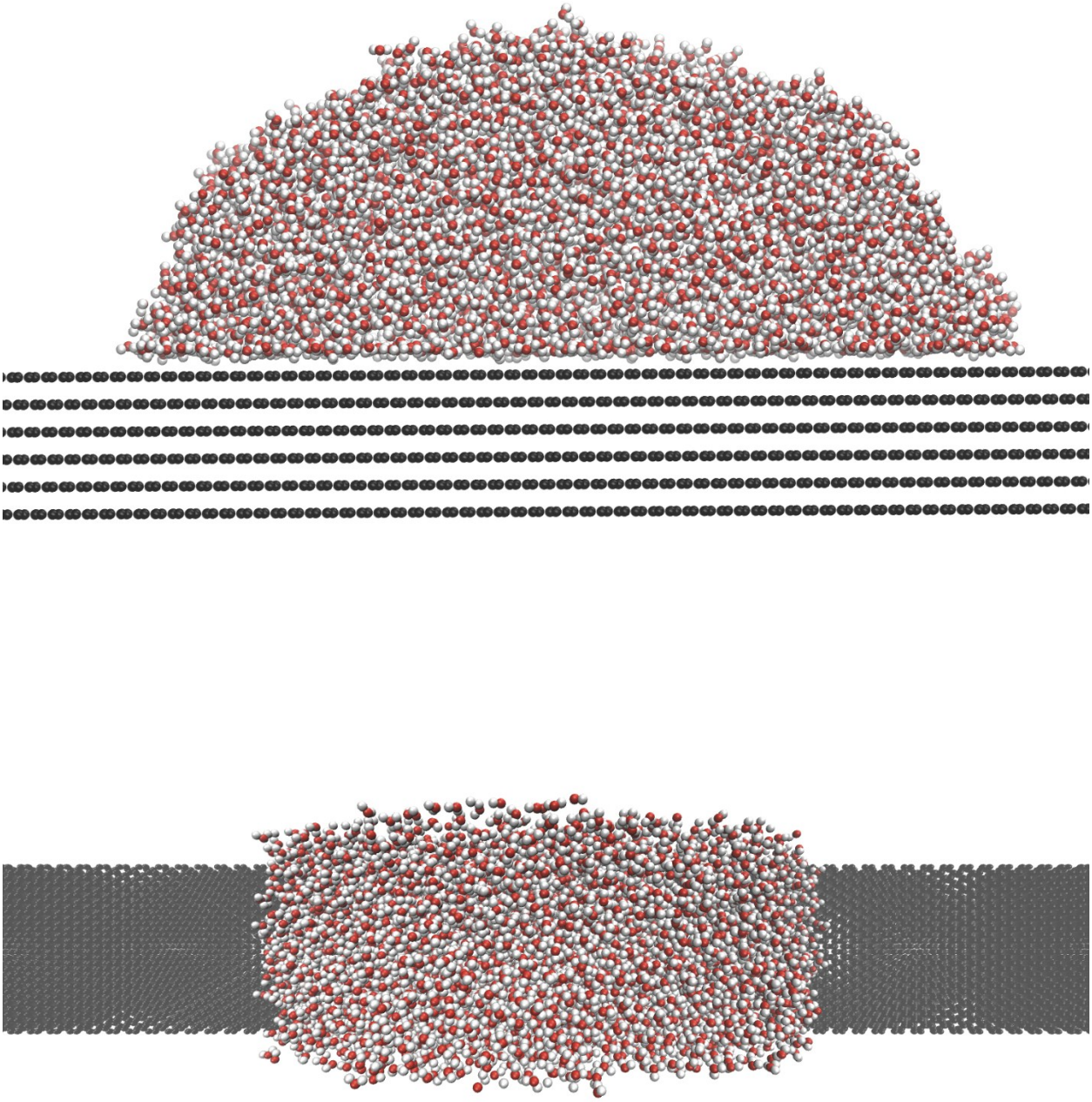

Figure S2: (Top) Side view of a snap shot of the equilibrated system and **(Bottom)** top view of the snap shot of the equilibrated system

The interaction between the water molecule and the underlying substrate is also modeled as a 12-6 LJ potential between the oxygen atoms and the substrate atoms. We use two sets of LJ parameters: a) derived by *Werder et. al,* [6] and, b) parameters derived from the All Atom Optimized potential for Liquid Simulations (OPLS-AA) [7]. The appropriate parameters for the different models used are listed in Table 2. In the case of epoxy terminated graphene, the terminal oxygen and carbon attached to the epoxy oxygen carry partial charge of Q_{OT} = - 0.28e and Q_{CT} = +0.14e due to the polar nature of the C-O bonds.

It has been shown that the total water-substrate interaction energy (U_{H2O-C}) directly affects the computed contact angle values in MD. Hence, it is important to calculate U_{H2O-C} accurately. For the same reason we set the cut-off for the water-substrate interaction as 20 Å. Accordingly, the thickness of the substrates used in our simulations were always between 20 Å and 25 Å since atoms deeper than 25 Å from the surface of the substrate do not contribute.

Table 2: LJ parameters from Werder et. al and OPLS-AA force field. The subscripts 'O', 'CG', 'CH', 'CT' and 'OT' refer to oxygen atom in water molecules, graphitic carbon, hydrogen termination at the graphene edges, carbon attached to an epoxy group at the graphene edges and oxygen in the epoxy group respectively.

	Parameters	**Value**
Werder et. al	ε_{O-CG}	0.392 kJ mol^{-1}
	σ_{O-CG}	3.190 Å
OPLS-AA	ε_{O-CG}	0.436 kJ mol^{-1}
	ε_{O-CH}	0.285 kJ mol^{-1}
	ε_{O-CT}	0.423 kJ mol^{-1}
	ε_{O-OT}	0.617 kJ mol^{-1}
	σ_{O-CG}	3.352 Å
	σ_{O-CH}	2.768 Å
	σ_{O-CT}	3.329 Å
	σ_{O-OT}	3.030 Å

The initial configuration (Figure S1a) is equilibrated under an NVT ensemble at 300 K using the Nosé–Hoover thermostat with a coupling constant of 10 fs. The time step of integration used in all our simulations is 1 fs. *Ma et. al* [8], showed that water nanodroplets on graphene sheet has a

high diffusion co-efficient due to the thermal ripples in graphene. Here, we keep the substrate atoms frozen and integrate the positions of only the water molecules. Such a simplification has been shown not to affect the resulting contact angle[6]. We still observe a non-negligible diffusion on the graphene sheets. Hence to compare against the experimental static contact angles, the linear momentum of the center of mass of the water droplet was reset to zero every 1 ps. All the data for the calculation of contact angle was sampled after the U_{H2O-C} and temperature converges to a constant value, *i.e.*, after equilibration. Figure S3 shows the convergence of U_{H2O-C} and temperature with time.

The mass density profile of the water droplet was obtained by dividing the simulation box into bins in the shape of pencils of uniform cross-section running parallel to the y-direction of the simulation box (Figure S4a). The mass density of water in each bin was averaged over a span of 1 ns to generate the mass-density profile (Figure S4b). The mass density profile of the water-droplet is further divided into slabs along the z direction. Figure S5 shows the mass-density at the center of the water droplet along the z direction. The peaks at the first few bins agrees with the typical ordering behavior of a fluid near a solid surface. In experiments, the macroscopic contact angle measured are at least a few tens of atomic layers away from the surface. We thus eliminate the data before the first two peaks. The following sigmoidal function is curve fitted over the mass density of each slab.

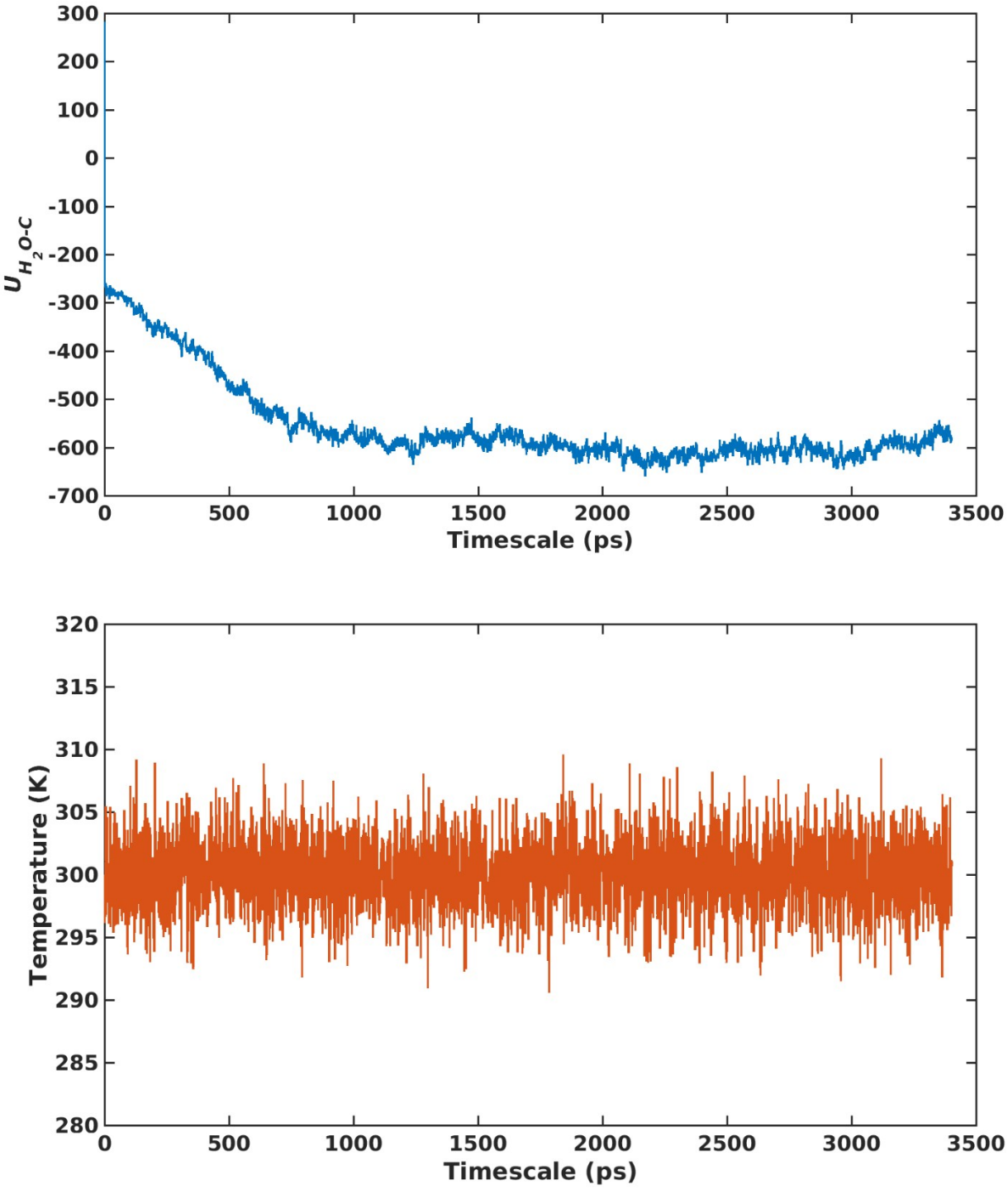

Figure S3: (Top) Evolution of the interaction energy between the water droplet and substrate with time. Convergence was achieved within 2.5 ns in all the cases. **(Bottom)** Temperature fluctuations are minimum and the system is well equilibrated under the thermostat.

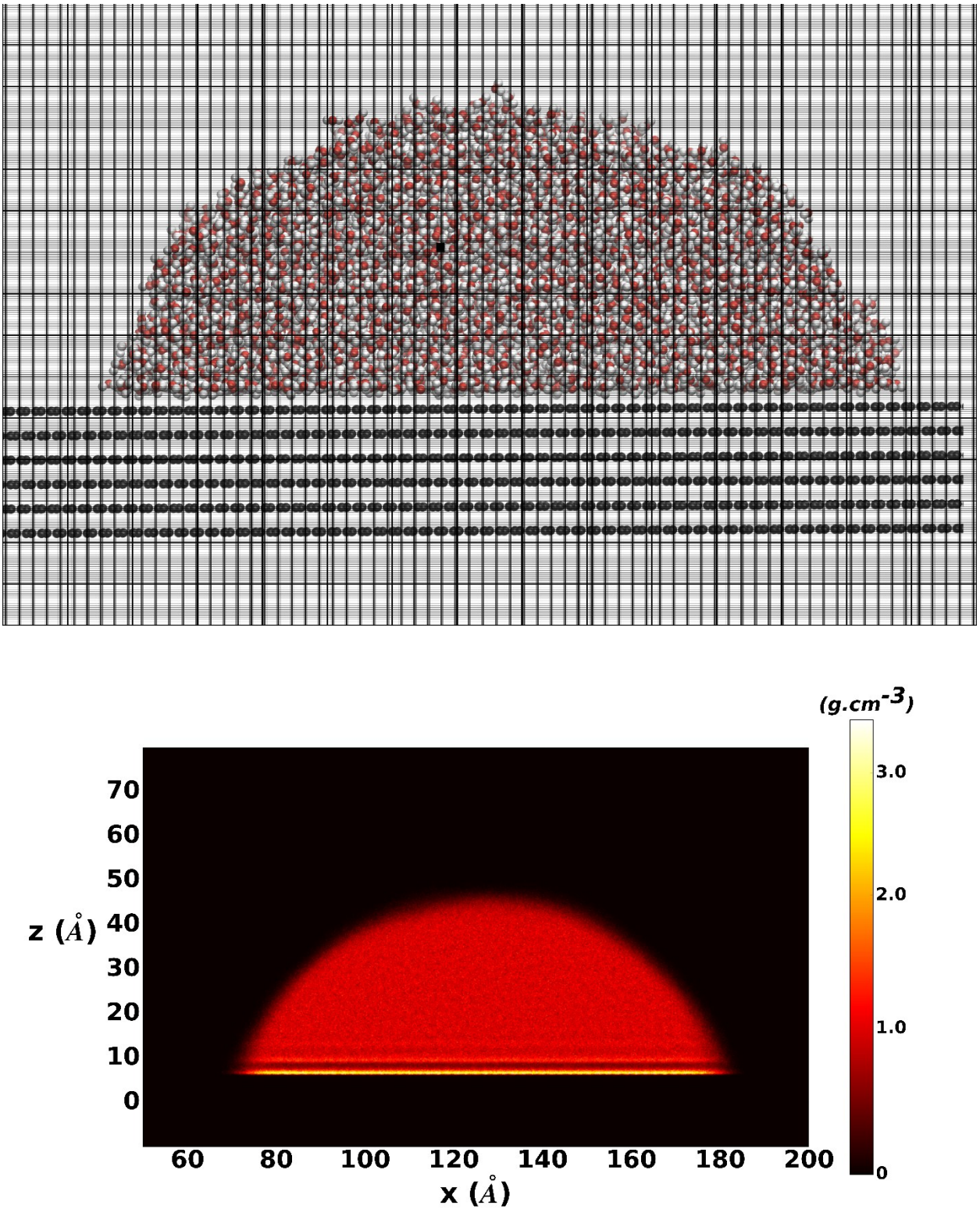

Figure S4: (Top) The simulation box is divided into bins, along the x-z plane, in the shape of pencils running parallel to the y-axis. **(Bottom)** The mass density in each bin is averaged over a

span of 1 ns to generate the density map. The cross section of the bins is used to generate this density map.

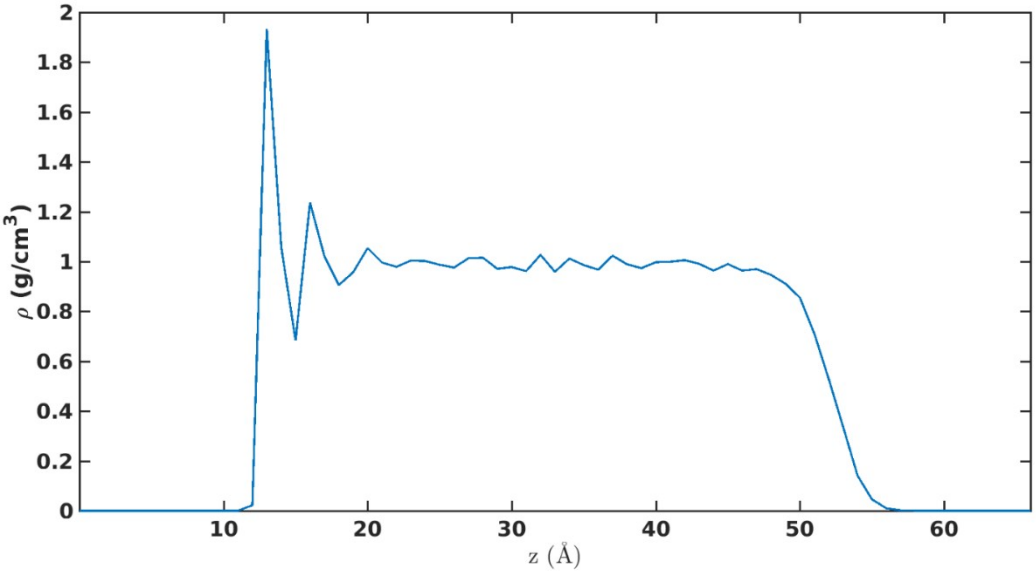

Figure S5: Mass density profile at the center of the droplet along the direction

$$\rho(r) = \frac{1}{2}(\rho_\beta(dr) + \rho_\beta(g)) - \frac{1}{2}(\rho_\beta(dr) - \rho_\beta(g))tanh\left(\frac{2(r - r_\beta)}{d_\beta}\right) \quad (1)$$

where r is the distance from the center of the water droplet, ρ is the mass-density, $\rho_\beta(dr)$ is the mass density in sheet β near the center of the water droplet, $\rho_\beta(g)$ is mass density of surrounding gas (assumed to be zero), r_β is the radius of the droplet in slab β, d_β is the thickness of the interface and Δz is the thickness of each slab. The contact angle is calculated as[9]:

$$\theta = \lim_{\Delta z \to 0} tan^{-1}\left(\frac{\Delta z}{r_2 - r_1}\right) \quad (2)$$

Where r_1 and r_2 are the radius of the water-droplet in the first two sheets considered.

Effect of stacking sequence on contact angle

All the simulations in our work were done with energetically favored AB stacking sequence of graphene. In order to investigate the effect of stacking sequence, we estimate the contact angle of

AA stacked vertically oriented graphene with Werder parameters. The results are compared against AB stacking in Table 3.

Table 3: Estimated CA's for graphene with AB and AA stacking respectively.

AB stacking	$\theta_c = 118.50$
AA stacking	$\theta_c = 118.79$

Effect of airborne hydrocarbon contamination

To determine the presence of airborne contaminants (such as hydrocarbons and moisture)[10] in the IPG, we conducted differential scanning calorimetry (DSC) as well as the mass loss experiments on two samples: unannealed IPG and IPG that was laser processed with 100 mJ/cm^2 energy density. In detail, the gas evolution from each of the samples was analyzed by heating it in a furnace in argon ambient whose output is connected to a mass spectrometer as well as to a DSC analyzer. The adsorbed gases in each of the samples were observed between 200^{o}C and 400^{o}C, confirming the airborne hydrocarbon contamination/adsorption on the sample surface (Fig. S6). Most likely such gas formation is mostly comprised of H_2O and CO_2 originating from hydrocarbon contamination/adsorption on the IPG surface as C-C bonds in the sp2 configuration are unlikely to break apart within this temperature range.

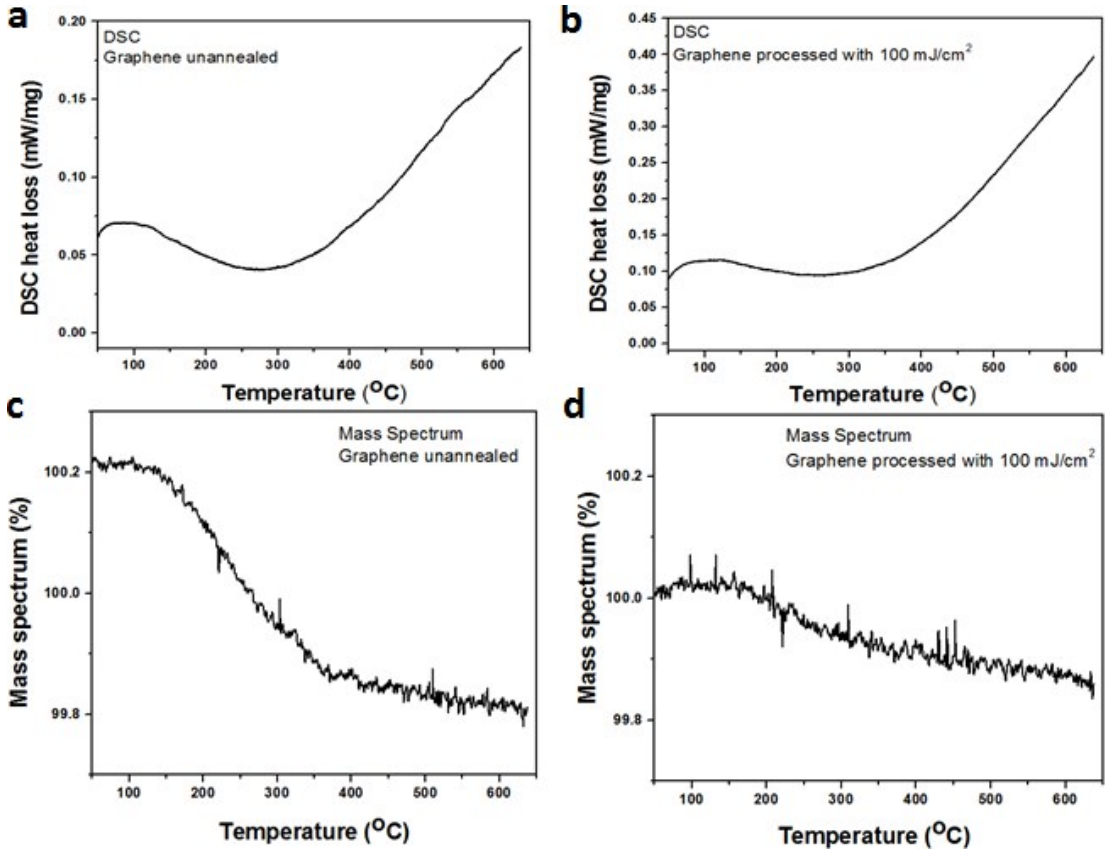

Figure S6: The heat loss and mass loss, caused by airborne hydrocarbon contamination, were studied on unannealed and laser annealed (at 100 mJ/cm^2) IPG that was printed on silicon/silicon dioxide substrates via (top row) differential scanning calorimetry (DSC) and measurement from (bottom row) a mass spectrometry.

Supplemental Video 1 Caption: Water droplets distinctly form on IPG treated with DPLW while not forming on an untreated region within an ESEM. The ESEM chamber humidity was set to ~100%, the pressure at 640 Pa, and the temperature was varied from 1.1°C down to 0.1°C to induce the water droplet formation.

REFERENCES:

1. J. Rafiee, X. Mi, H. Gullapalli, A. V. Thomas, F. Yavari, Y. Shi, P. M. Ajayan and N. A. Koratkar, *Nat. Mater.*, 2012, **11**, 217-222.
2. G. Scocchi, D. Sergi, C. D'Angelo and A. Ortona, *Physical Review E*, 2011, **84**, 061602.
3. H. J. C. Berendsen, J. R. Grigera and T. P. Straatsma, *The Journal of Physical Chemistry*, 1987, **91**, 6269-6271.
4. R. W. Hockney and J. W. Eastwood, *Computer simulation using particles*, Taylor \& Francis, Inc., 1988.
5. I.-C. Yeh and M. L. Berkowitz, *The Journal of Chemical Physics*, 1999, **111**, 3155-3162.
6. T. Werder, J. H. Walther, R. L. Jaffe, T. Halicioglu and P. Koumoutsakos, *The Journal of Physical Chemistry B*, 2003, **107**, 1345-1352.

7. W. L. Jorgensen, D. S. Maxwell and J. Tirado-Rives, *Journal of the American Chemical Society*, 1996, **118**, 11225-11236.
8. M. Ma, G. Tocci, A. Michaelides and G. Aeppli, *Nat Mater*, 2016, **15**, 66-71.
9. T. Ingebrigtsen and S. Toxvaerd, *The Journal of Physical Chemistry C*, 2007, **111**, 8518-8523.
10. Z. Li, Y. Wang, A. Kozbial, G. Shenoy, F. Zhou, R. McGinley, P. Ireland, B. Morganstein, A. Kunkel, S. P. Surwade, L. Li and H. Liu, *Nat Mater*, 2013, **12**, 925-931.